Hindawi Publishing Corporation
International Journal of Polymer Science
Volume 2016, Article ID 9351725, 8 pages
http://dx.doi.org/10.1155/2016/9351725

Research Article

Synthesis and Characterization of Uniform Spherical Nanoporous TiO_2 Aerogel Templated by Cellulose Alcohol-Gel with Enhanced Photocatalytic Activity

Zhiming Liu,[1] Peng Wu,[1] Shaoli Yang,[1] Haiying Wang,[1] and Chunde Jin[2]

[1]*Northeast Forestry University, Harbin 150040, China*
[2]*Zhejiang Agriculture and Forestry University, Hangzhou 311300, China*

Correspondence should be addressed to Zhiming Liu; zhimingliuwhy@126.com

Received 3 March 2016; Accepted 26 April 2016

Academic Editor: Zhouyang Xiang

The spherical nanoporous TiO_2 aerogels were prepared by a simple ethanol-thermal method, using spherical cellulose alcohol-gel as the template. The morphology, crystalline structure, pore size, specific surface area, and the photocatalytic activity of obtained TiO_2 aerogel were separately characterized by scanning electron microscopy (SEM), transmission electron microscopy (TEM), X-ray diffraction (XRD), X-ray photoelectron spectroscopy (XPS), N_2 adsorption-desorption isotherms, and double beam UV-VIS spectrophotometer. The characteristics of TiO_2 aerogels presented uniform sphere shape, good internal structural morphology, high specific surface area (ranging from 111.88 to 149.95 m^2/g), and good crystalline anatase phase. Moreover, methyl orange dye was used as the target pollutant to characterize the photocatalytic activities and the adsorption performance. The photocatalytic experiment shows that the obtained spherical TiO_2 aerogels had a higher degradation ratio of 92.9% on methyl orange dye compared with aspherical TiO_2 aerogels prepared from other concentrations of tetrabutyl orthotitanate (TBOT).

1. Introduction

In the early 1990s, the ordered mesoporous silica was found for the first time [1, 2]. Since then, mesoporous materials have become one of the most important materials for catalysis [3–5]. With the fascinating properties of high specific surface areas, tunable large pore sizes, large pore volumes, controllable framework compositions, and alternative pore shapes, mesoporous materials can also be used in drug delivery, separation, sorption, fuel cells, gas separators, and magnetism areas [6–8]. Recently, researchers have paid much more attention to the mesoporous materials, such as TiO_2, ZnO, and SnO_2, which have the photocatalytic oxidation abilities to degrade the organic pollutants in water and air [9–11].

Among various oxide semiconductor photocatalysts, TiO_2 has successfully attracted a great deal of interest and also has been the most promising photocatalyst due to its strong oxidizing potential, the low cost, high chemical stability against photocorrosion, and excellent degradation for organic pollutants [12, 13]. However, practical applications of titanium dioxide are still quite limited, mainly because of its low quantum efficiency and the broad bandgap which responds only to UV light [14]. In addition to the VB position, the pore configuration and particle size distribution of photocatalyst also influence the activity of a photocatalyst. In order to obtain nanoporous structure and high dispersibility of TiO_2, there are three approaches: the template synthesis [15–19], the anodic oxidation [20–22], and the hydrothermal synthesis [23–25]. Among those, the template-based synthesis route takes the advantage of straightforward controlling over the morphology of the resulting TiO_2 nanoporous structured materials and maintaining TiO_2 good disperse stability on the surface of the template [19]. Recently, cellulose fiber has been used as a template to synthesize nanoporous structured materials, such as TiO_2, CdS, and Fe_2O_3. Furthermore, cellulose alcohol-gel or hydrogel not only takes over cellulose fiber's excellent characteristics, including high tensile strength, high water holding capacity, high crystallinity, and good biocompatibility but also generates the dimensional and porous structure and the uniform nanopore size [26].

The unique structure of cellulose aerogel bestows it on unusual properties. Herein we reported our research work in the preparation of spherical nanoporous TiO_2 aerogel using spherical cellulose aerogel as the host matrix, employing tetrabutyl orthotitanate (TBOT), urea, and dehydrated alcohol as the starting materials. The resulting TiO_2 spheres were characterized by transmission electron microscopy (TEM), X-ray diffraction (XRD), and the nitrogen gas adsorption (Micromeritics, ASAP 2020 analyzer) techniques. The influence of the concentration of TBOT on the morphologies and size of TiO_2 nanoparticles was investigated. Meanwhile, the excellent photocatalytic activity for the degradation of methyl orange dye (MO) in aqueous solution was also demonstrated under UV irradiation at room temperature. We hope to provide a novel method for easily creating nanoporous TiO_2 aerogel. Our findings may provide a new and "green" pathway for the design and fabrication of photocatalytic materials to solve the problem of organic pollution.

2. Materials and Methods

2.1. Materials. The commercial natural bamboo fiber, which was manufactured by slicing, steaming, cooking, and enzymatic process, was used as raw materials for preparation of spherical cellulose alcohol-gels. The fiber with 1.5 D (denier) and 38 mm length was purchased from Mingtong Bamboo Charcoal Products Co., Ltd., China. All other chemicals were of analytical grade and used without further purification.

2.2. Preparation of Spherical Cellulose Alcohol-Gels. The spherical cellulose alcohol-gels were synthesized using the hand-dropping procedure as follows. A solution with NaOH/urea/H_2O of 7 : 12 : 81 (mass ratio) was cooled to −12°C as solvent system. 2.0 g natural bamboo cellulose fiber was dispersed into 100 g solvent system under vigorous stirring to obtain the transparent cellulose solution. Then, the cellulose solutions were added drop by drop to the well-mixed regenerate solution with a certain proportion of trichloropropane, ethyl acetate, and acetic and solidified at room temperature for 10 min before rinsing under running deionized water for 12 h. Finally, the spherical cellulose alcohol-gels were obtained after adequate exchanging for several times with ethanol.

2.3. Preparation of Spherical TiO_2 Aerogels. The spherical TiO_2 aerogels were prepared by an ethanol-thermal method. Firstly, 0.1 g of urea was added to a 100 mL beaker with 40 mL of anhydrous ethanol under magnetic stirring. Meanwhile, 0.1 mL of TBOT was put into the mixed solution. When TBOT mixed the urea and anhydrous ethanol, 1.0 g of spherical cellulose alcohol-gels was added into the solution. After placing it for 2 h to form sol-gel at room temperature, the final reactant was transferred into a 50 mL Teflon-lined stainless steel autoclave through heat treatment at 120°C for 10 h. Then the products were separately washed with deionized water, ethanol, and t-butyl alcohol three times every day for two days and freeze-dried overnight at 30–40 Pa of vacuum. Finally, the TiO_2 with spherical cellulose aerogel template was calcined in oxygen atmosphere at 500°C for 3 h (heating rate: 1°C/min). Similarly, various nanoporous TiO_2 aerogels prepared from 0.5 mL and 5 mL of TBOT were also synthesized for comparison while the other experimental conditions were not changed.

2.4. Characterization of Spherical TiO_2 Aerogels. The morphology of spherical TiO_2 aerogels was observed on the scanning electron microscopy (SEM; Quanta 200, FEI, Hillsboro, OR, USA) and the transmission electron microscopy (TEM; JEOL 2011, FEI Holland). X-ray diffraction (XRD) patterns of spherical TiO_2 aerogels were measured by a Rigaku D/Max-rB diffractometer (Tokyo, Japan) with Cu-Kα radiation (45 kV, 40 mA, λ = 1.54178 Å) ranging from 4° to 90° (2θ angle). The pore size and the BET specific surface areas of the samples were calculated using N_2 adsorption-desorption isotherms measured at −196°C with an ASAP 2020 instrument (Micromeritics, American). The elemental compositions and states were tested by X-ray photoelectron spectroscopy (XPS, Chanhassen, MN, USA) with Al-Kα radiation ($h\nu$ = 1486.6 eV).

2.5. Photocatalytic Experiment. The photocatalytic activities of the spherical nanoporous TiO_2 aerogel were investigated in terms of the photocatalytic degradation of 10 mg/L methyl orange dye (MO) solution under illumination of UV light at 254 nm. Before the illumination, 50 mg of the spherical TiO_2 aerogels was first added to photocatalytic device filled with 150 mL of 10 mg/L MO, and the mixture was stirred for 30 min to reach a saturated state. Simultaneously, the adsorption/desorption of MO and O_2 molecules on the spherical TiO_2 aerogels surface reached an equilibrium in the darkness. Then the stirring solution was illuminated by the vertically incident UV light. During the photocatalytic reaction, samples were carried from the supernatant solution at every 15 min and were immediately centrifuged at 2000 r/min for 5 min. The concentration of MO after catalyzing was measured by a TU-1901 UV-visible spectrometer at 460 nm.

3. Results and Discussion

3.1. Morphology Analysis. Figure 1 shows the photographs of TiO_2 aerogel prepared from different concentrations of TBOT. With the increasing concentration of TBOT, TiO_2 aerogel was shifted to spherical structure, and these TiO_2 aerogels had the uniform shapes showed in Figure 1(c). For the morphology of TiO_2 aerogel, the cellulose alcohol-gel played a role of template and morphology guiding in the preparation of nanoporous TiO_2 aerogel.

To observe the internal structure of the TiO_2 aerogel, these TiO_2 aerogels were broken into two parts, and the surface of the fracture surface could be imaged by scanning electron microscopy (SEM). Figures 2(a)–2(c), respectively, represented morphology of TiO_2 aerogel prepared from different concentrations of TBOT. The formation of the network structure of TiO_2 aerogel could be attributed to the accumulation of the TiO_2 nanoparticles. When the concentration of TBOT was increasing, the network structure

Figure 1: Photographs of TiO_2 aerogel: (a) aspherical TiO_2 aerogel-0.1 mL of TBOT, (b) aspherical TiO_2 aerogel-0.5 mL of TBOT, and (c) spherical TiO_2 aerogel-5.0 mL of TBOT.

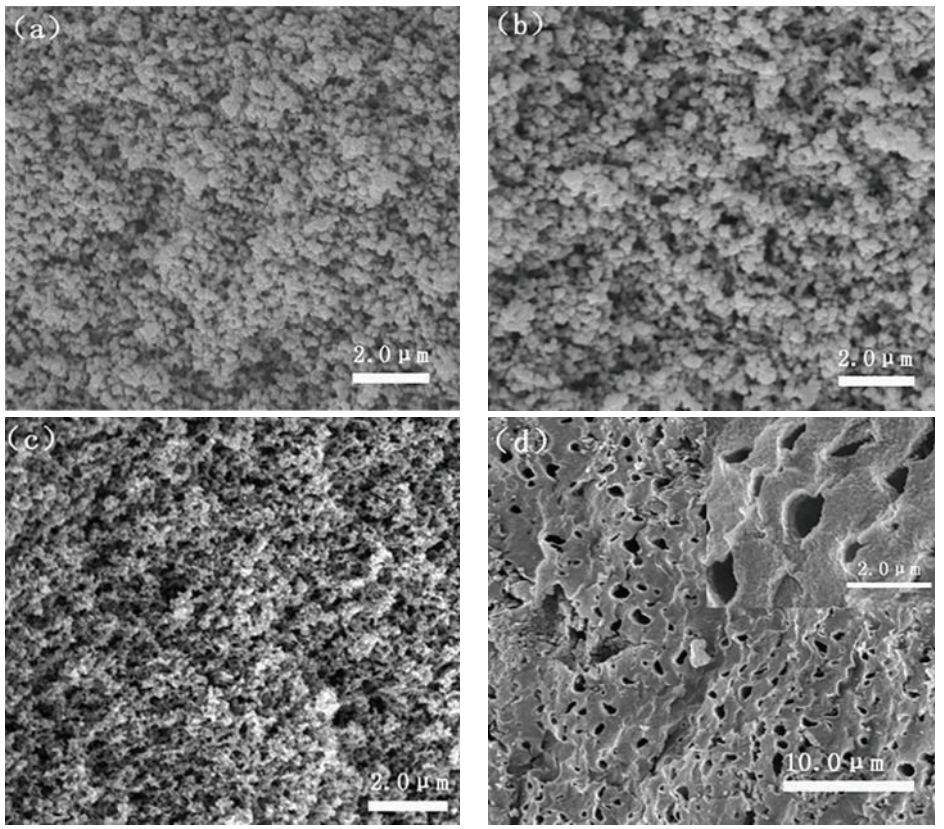

Figure 2: SEM images of TiO_2 aerogel: (a) internal structure of aspherical TiO_2 aerogel-0.1 mL of TBOT, (b) internal structure of aspherical TiO_2 aerogel-0.5 mL of TBOT, (c) internal structure of spherical TiO_2 aerogel-5.0 mL of TBOT, and (d) external surface structure of spherical TiO_2 aerogel.

of TiO_2 aerogel was more obvious. Moreover, the external surface of spherical TiO_2 aerogel was filled with pores shown in Figure 2(d). These pores mainly inherited the porosity of spherical cellulose aerogels matrix while the spherical TiO_2-cellulose complex aerogel was calcined. Detailed information concerning the pore size and the specific surface area was analyzed in pore structure.

The TEM images of these TiO_2 aerogels were shown in Figure 3. The shape of TiO_2 particle prepared from 0.1 mL of TBOT was irregular and the agglomeration could be clearly

Table 1: Specific surface area and pore structure parameters of TiO_2 aerogel prepared from different concentrations of TBOT.

Samples	S_{BET} (m^2/g)	Mesoporous volume (cm^3/g)	Average pore diameter (nm)
TiO_2-0.1 mL of TBOT	129.32	0.52	16.20
TiO_2-0.5 mL of TBOT	111.88	0.42	15.04
TiO_2-5.0 mL of TBOT	149.95	0.49	12.96

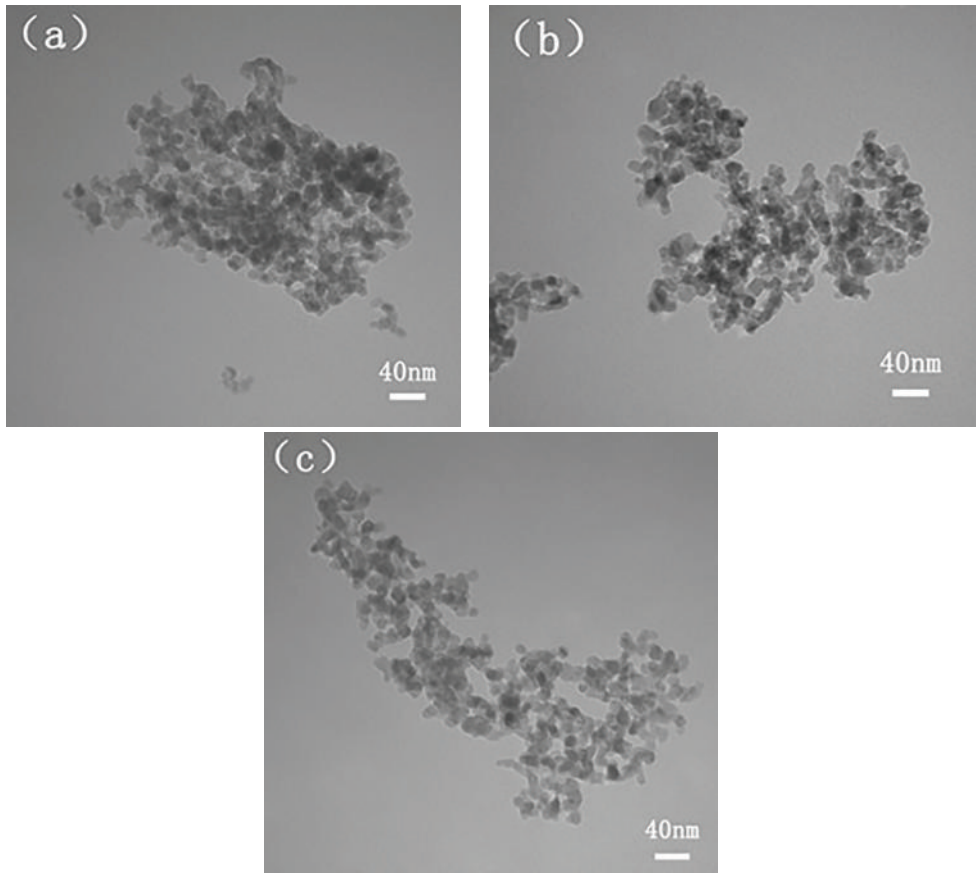

Figure 3: TEM images of TiO_2 aerogel: (a) aspherical TiO_2 aerogel-0.1 mL of TBOT, (b) aspherical TiO_2 aerogel-0.5 mL of TBOT, and (c) spherical TiO_2 aerogel-5.0 mL of TBOT.

observed in Figure 3(a). But when the concentration of TBOT was added to 0.5 mL of TBOT, the TiO_2 particle's shape was almost in conformity and had minor agglomeration shown in Figure 3(b). The shape of TiO_2 particle was uniform sphere and scarcely had agglomeration until the concentration of TBOT was up to 5.0 mL, which was shown in Figure 3(c). Furthermore, the diameter of TiO_2 particle was about 15–20 nm, implying that the single TiO_2 particle that consisted of TiO_2 aerogel was nanoparticle.

3.2. Pore Structure. Figure 4 shows nitrogen adsorption-desorption curves (inset) and corresponding pore-size distribution of TiO_2 aerogel prepared from different concentrations of TBOT. The isotherms were measured to be Type IV, according to the IUPAC classification. The hysteresis loops were obviously observed at P/P_0 = 0.8–1.0, and the shapes of these hysteresis loops conformed to H3 hysteresis loops, indicating that obtained TiO_2 aerogels were mesoporous materials [27–30]. The pore-size distribution results show that every sample had a bimodal distribution (2-3 nm and 10–100 nm), and the peak pore was around 2.3 nm and 34 nm. The different diameters of the pores may result from the different stacking styles of the TiO_2 particles, which were confirmed by SEM.

Detailed information in terms of the specific surface areas and the porosities of the TiO_2 aerogels was summarized in Table 1. With the increasing concentration of TBOT, the shape of the TiO_2 aerogel was shifted to sphere, leading to an increase in the specific surface areas and a drop in the pore size. When the consumption of TBOT was 5.0 mL, the specific surface area of obtained TiO_2 aerogel can reach 149.95 m^2/g, and the corresponding pore size was 12.96 nm. In addition, the increased specific area of spherical TiO_2 aerogel compared with the aspheric TiO_2 aerogels mainly came from these mesoporous areas, which agreed with the pore volume and pore-size distributions.

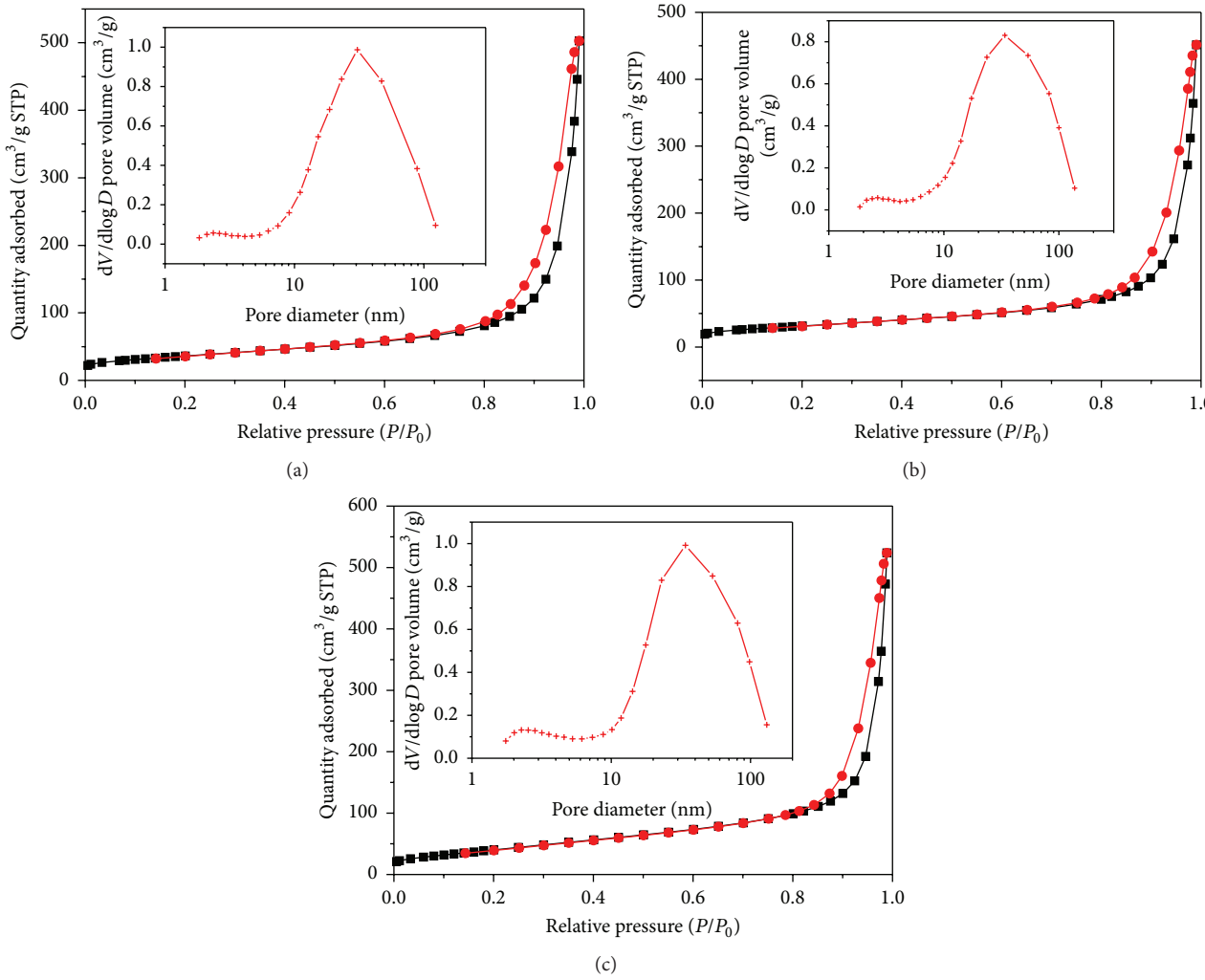

FIGURE 4: N_2 adsorption-desorption isotherm curves and corresponding pore-size distribution of (a) aspherical TiO_2 aerogel-0.1 mL of TBOT, (b) aspherical TiO_2 aerogel-0.5 mL of TBOT, and (c) spherical TiO_2 aerogel-5.0 mL of TBOT.

3.3. XRD and XPS Results. The X-ray diffraction (XRD) patterns of TiO_2 aerogel are shown in Figure 5. With the increasing concentration of TBOT, the (101) peak position of TiO_2 aerogel shifted to the higher-angle region shown in Figure 5(a). And the obvious characteristic diffraction peaks of TiO_2 aerogel could be seen in Figure 5(b), which was attributed to anatase TiO_2 crystals [31]. No peaks from other impurities were detected in this XRD pattern. Furthermore, the strong and sharp diffraction peaks shown in Figure 5 indicated that the obtained spherical TiO_2 aerogel had high crystallinity [32].

The chemical compositions and elemental environments of the catalysts were tested by X-ray photoelectron spectroscopy (XPS); the specific spectra are shown in Figure 6. Three elements, Ti, O, and C, were revealed in Figure 6(a). Among them, the existence of C elements may result from trace organic pollutants in the vacuum measurement of XPS instrument. High-resolution spectra of Ti 2p and O 1s region were separately shown in Figures 6(b) and 6(c). The obvious peaks, where binding energies were 458.59 eV and 464.34 eV, were the characteristic peaks of Ti $2p_{1/2}$ and Ti $2p_{3/2}$. Furthermore, the binding energy of Ti $2p_{1/2}$ was 5.75 eV lower than that of Ti $2p_{3/2}$, which was the important criterion of existence of Ti^{4+} [33, 34]. Figure 6(c) shows the XPS spectra of O 1s with a broad and asymmetrical peak, suggesting that the oxygen species on the surface of spherical TiO_2 aerogel was not a single species. The O 1s region could be fitted with three peaks, whose binding energies were 529.78, 531.11, and 531.98 eV. These peaks were in accordance with the binding energy data of lattice oxygen, hydroxyl, and physically adsorbed oxygen [35]. O 1s mainly existed as lattice oxygen in Ti-O-Ti bonds observed from the areas of the peaks. This reveals that the obtained spherical TiO_2 aerogel consisted of titania and some Ti-OH generated in the reaction process [35].

3.4. Photocatalytic Activity. The photocatalytic activities of the spherical nanoporous TiO_2 aerogel were investigated in terms of the photocatalytic degradation of 10 mg/L MO

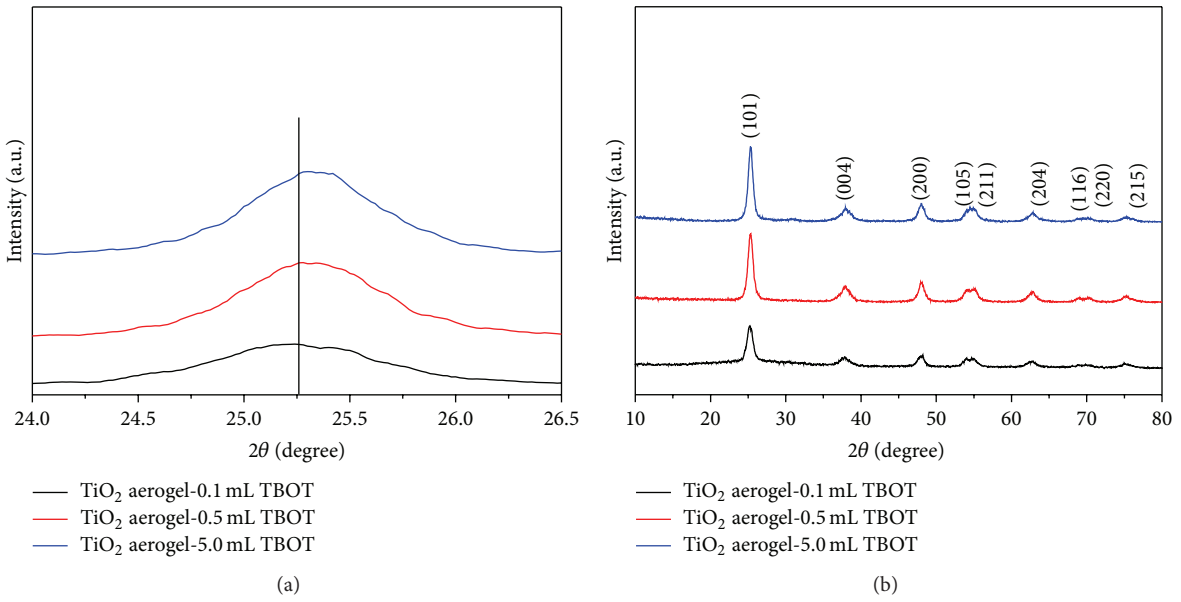

FIGURE 5: XRD patterns of Ti diffraction peak at $2\theta = 25.26^{\circ}$ (a) and TiO_2 aerogels calcinated at 500°C for 3 h.

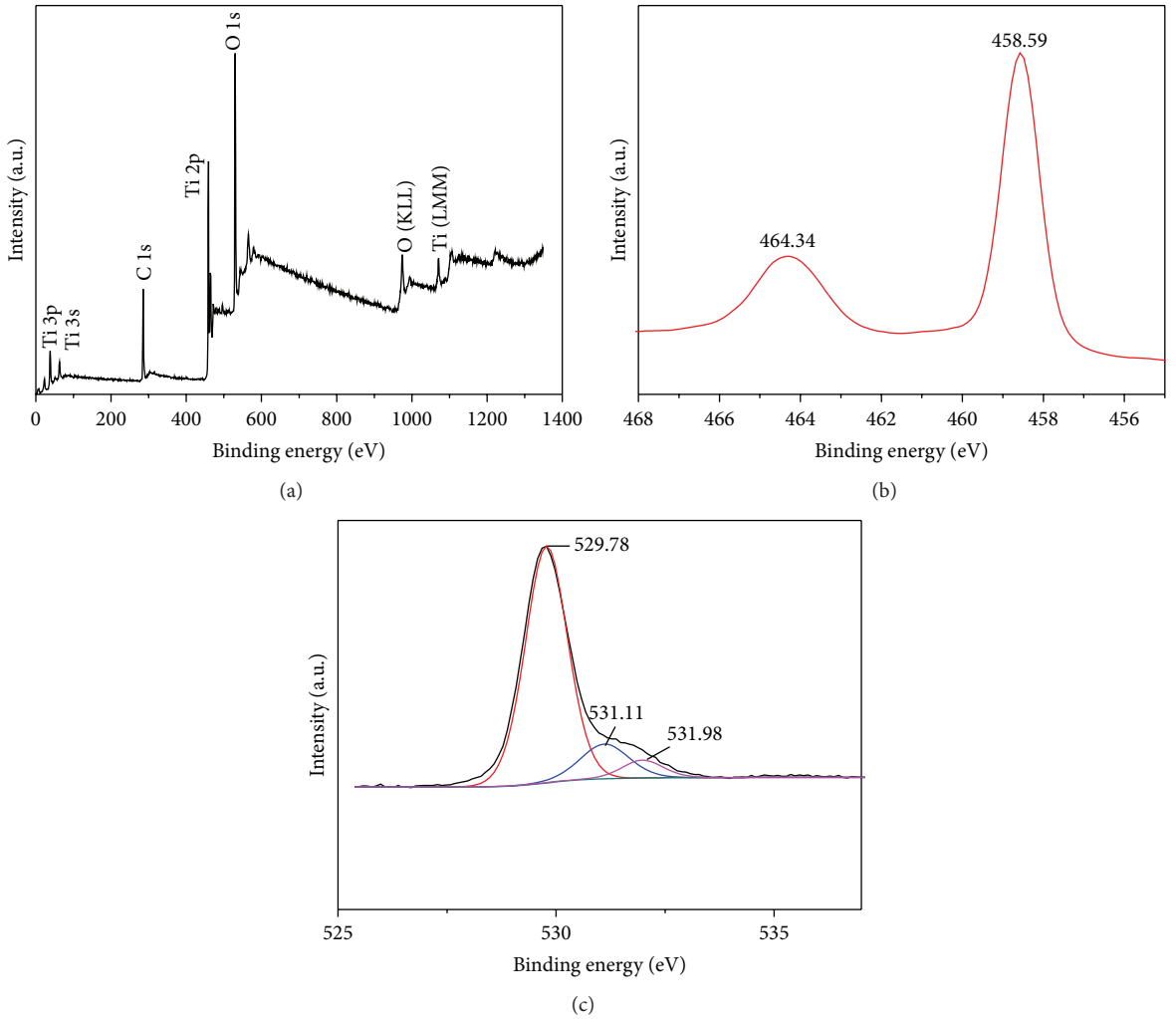

FIGURE 6: XPS spectra of TiO_2 aerogel (a) total spectrum; high-resolution spectrum of the (b) Ti 2p and (c) O 1s region.

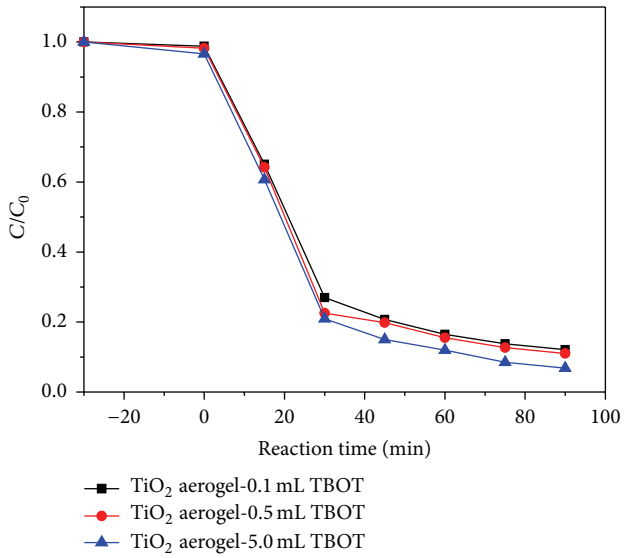

Figure 7: The degradation curves of MO in the presence of the TiO_2 aerogels prepared from 0.1 mL of TBOT, 0.5 mL of TBOT, and 0.5 mL of TBOT.

under illumination of UV light within 90 min (Figure 7). As a control, the activities of aspherical TiO_2 aerogels were also examined under the same conditions. Results of the photocatalytic investigation are shown in Figure 7. Obviously, the photocatalytic activity of spherical TiO_2 aerogel prepared from 5.0 mL of TBOT was higher than the aspherical TiO_2 aerogels prepared from 0.1 mL of TBOT and 0.5 mL of TBOT. In the process of adsorption equilibrium, the first reaction time of 30 min, the removal rate of MO with the spherical TiO_2 aerogels was higher than that of aspherical TiO_2 aerogels. This phenomenon may result from the fact that spherical TiO_2 aerogels had the higher specific surface area than aspherical TiO_2 aerogels. Moreover, with the increase in degradation time, the concentration of MO decreased rapidly, and, after 90 min of irradiation, the decomposition ratio of MO over the spherical TiO_2 aerogels prepared from 5.0 mL of TBOT was about 92.9%, while those of aspherical TiO_2 aerogels prepared from 0.1 mL and 0.5 mL of TBOT were 87.8% and 88.8%. Therefore, both the spherical TiO_2 aerogels and the aspherical TiO_2 aerogels had excellent photocatalytic activity of MO, which can be attributed to special anatase phase, specific surface areas, and unique structure [7].

4. Conclusions

Spherical TiO_2 aerogels were prepared by a simple ethanol-thermal method, using spherical cellulose aerogel as the template and TBOT as raw material. The obtained TiO_2 aerogels consisted of TiO_2 nanoparticles with the diameter 15–20 nm. The high specific surface area, ranging from 111.88 m^2/g to 149.95 m^2/g, and good porosity of the network structures provided a large number of active sites for photocatalysis. The highest UV light activity, giving methyl orange degradation of 92.9%, was achieved by spherical TiO_2 aerogel prepared from 5.0 mL of TBOT under the calcination condition of 500°C for 3 h.

Competing Interests

The authors declare that there are no competing interests regarding the publication of this paper.

Acknowledgments

This research was financially supported by the Industry Research Special Funds for Public Welfare Project under Grant no. 201504602, the Key Laboratory of Wood Science and Technology, Zhejiang Province, under Grant no. 2014lygcz002, and the Fundamental Research Funds for the Central Universities under Grant no. 2572014EB01-02. Special thanks are due to Professor Shujun Li for her equipment and analysis.

References

[1] A. A. Ismail and D. W. Bahnemann, "Mesoporous titania photocatalysts: preparation, characterization and reaction mechanisms," *Journal of Materials Chemistry*, vol. 21, no. 32, pp. 11686–11707, 2011.

[2] R. Y. Zhang, A. A. Elzatahry, S. S. Al-Deyab, and D. Zhao, "Mesoporous titania: from synthesis to application," *Nano Today*, vol. 7, no. 4, pp. 344–346, 2012.

[3] J. L. Vivero-Escoto, Y.-D. Chiang, K. C.-W. Wu, and Y. Yamauchi, "Recent progress in mesoporous titania materials: adjusting morphology for innovative applications," *Science and Technology of Advanced Materials*, vol. 13, no. 1, Article ID 013003, 2012.

[4] L. P. Kumaresan, A. Prabhu, M. Palanichamy, E. Arumugam, and V. Murugesan, "Synthesis and characterization of Zr^{4+}, La^{3+} and Ce^{3+} doped mesoporous TiO_2: evaluation of their photocatalytic activity," *Journal of Hazardous Materials*, vol. 186, no. 2-3, pp. 1183–1192, 2011.

[5] L. Kumaresan, A. Prabhu, M. Palanichamy, and V. Murugesan, "Synthesis of mesoporous TiO_2 in aqueous alcoholic medium and evaluation of its photocatalytic activity," *Materials Chemistry and Physics*, vol. 126, no. 1-2, pp. 445–452, 2011.

[6] P. Wang, J. Wang, X. F. Wang et al., "One-step synthesis of easy-recycling TiO_2-rGO nanocomposite photocatalysts with enhanced photocatalytic activity," *Applied Catalysis B: Environmental*, vol. 132-133, pp. 452–459, 2013.

[7] J. F. Ye, W. Liu, J. G. Cai et al., "Nanoporous anatase TiO_2 mesocrystals: additive-free synthesis, remarkable crystalline-phase stability, and improved lithium insertion behavior," *Journal of the American Chemical Society*, vol. 133, no. 4, pp. 933–940, 2011.

[8] J. G. Yu, W. Liu, and H. G. Yu, "A one-pot approach to hierarchically nanoporous titania hollow microspheres with high photocatalytic activity," *Crystal Growth and Design*, vol. 8, no. 3, pp. 930–934, 2008.

[9] Y. Liu, H. B. Jin, S. M. Zhu et al., "A facile method for fabricating TiO2 @ mesoporous carbon and three-layered nanocomposites," *Nanotechnology*, vol. 23, no. 32, Article ID 325602, 2012.

[10] B. Cheng, Y. Le, and J. Yu, "Preparation and enhanced photocatalytic activity of Ag@TiO_2 core-shell nanocomposite nanowires," *Journal of Hazardous Materials*, vol. 177, no. 1–3, pp. 971–977, 2010.

[11] E. J. W. Crossland, N. Noel, V. Sivaram, T. Leijtens, J. A. Alexander-Webber, and H. J. Snaith, "Mesoporous TiO_2 single

crystals delivering enhanced mobility and optoelectronic device performance," *Nature*, vol. 495, no. 7440, pp. 215–219, 2013.

[12] A. L. Linsebigler, G. Q. Lu, and J. T. Yates Jr., "Photocatalysis on TiO_2 surfaces: principles, mechanisms, and selected results," *Chemical Reviews*, vol. 95, no. 3, pp. 735–758, 1995.

[13] R. Asahi, T. Morikawa, T. Ohwaki, K. Aoki, and Y. Taga, "Visible-light photocatalysis in nitrogen-doped titanium oxides," *Science*, vol. 293, no. 5528, pp. 269–271, 2001.

[14] Z. Yanqing, S. Erwei, C. Zhizhan, L. Wenjun, and H. Xingfang, "Influence of solution concentration on the hydrothermal preparation of titania crystallites," *Journal of Materials Chemistry*, vol. 11, no. 5, pp. 1547–1551, 2001.

[15] D. Eder and A. H. Windle, "Morphology control of CNT-TiO_2 hybrid materials and rutile nanotubes," *Journal of Materials Chemistry*, vol. 18, no. 17, pp. 2036–2043, 2008.

[16] D. Eder, M. S. Motta, I. A. Kinloch, and A. H. Windle, "Anatase nanotubes as support for platinum nanocrystals," *Physica E*, vol. 37, no. 1-2, pp. 245–249, 2007.

[17] D. Eder, I. A. Kinloch, and A. H. Windle, "Pure rutile nanotubes," *Chemical Communications*, no. 13, pp. 1448–1450, 2006.

[18] D. Eder and A. H. Windle, "Carbon-inorganic hybrid materials: the carbon-nanotube/TiO_2 interface," *Advanced Materials*, vol. 20, no. 9, pp. 1787–1793, 2008.

[19] N. Bouazza, M. Ouzzine, M. A. Lillo-Ródenas, D. Eder, and A. Linares-Solano, "TiO_2 nanotubes and CNT-TiO_2 hybrid materials for the photocatalytic oxidation of propene at low concentration," *Applied Catalysis B: Environmental*, vol. 92, no. 3-4, pp. 377–383, 2009.

[20] Y. S. Sohn, Y. R. Smith, M. Misra, and V. (Ravi) Subramanian, "Electrochemically assisted photocatalytic degradation of methyl orange using anodized titanium dioxide nanotubes," *Applied Catalysis B: Environmental*, vol. 84, no. 3-4, pp. 372–378, 2008.

[21] R. P. Antony, T. Mathews, A. Dasgupta, S. Dash, A. K. Tyagi, and B. Raj, "Rapid breakdown anodization technique for the synthesis of high aspect ratio and high surface area anatase TiO_2 nanotube powders," *Journal of Solid State Chemistry*, vol. 184, no. 3, pp. 624–632, 2011.

[22] A. Tighineanu, T. Ruff, S. Albu, R. Hahn, and P. Schmuki, "Conductivity of TiO_2 nanotubes: influence of annealing time and temperature," *Chemical Physics Letters*, vol. 494, no. 4–6, pp. 260–263, 2010.

[23] B. D. Yao, Y. F. Chan, X. Y. Zhang, W. F. Zhang, Z. Y. Yang, and N. Wang, "Formation mechanism of TiO_2 nanotubes," *Applied Physics Letters*, vol. 82, no. 2, pp. 281–283, 2003.

[24] R. Yoshida, Y. Suzuki, and S. Yoshikawa, "Syntheses of TiO_2(B) nanowires and TiO_2 anatase nanowires by hydrothermal and post-heat treatments," *Journal of Solid State Chemistry*, vol. 178, no. 7, pp. 2179–2185, 2005.

[25] G. Mogilevsky, Q. Chen, A. Kleinhammes, and Y. Wu, "The structure of multilayered titania nanotubes based on delaminated anatase," *Chemical Physics Letters*, vol. 460, no. 4–6, pp. 517–520, 2008.

[26] S. Y. Chen, B. H. Zhou, W. L. Hu, W. Zhang, N. Yin, and H. Wang, "Polyol mediated synthesis of ZnO nanoparticles templated by bacterial cellulose," *Carbohydrate Polymers*, vol. 92, no. 2, pp. 1953–1959, 2013.

[27] F. Liu, J. Lu, J. Shen, and Z. Zhang, "Preparation of mesoporous nickel oxide of sheet particles and its characterization," *Materials Chemistry and Physics*, vol. 113, no. 1, pp. 18–20, 2009.

[28] M. Q. Chu and G. J. Liu, "Synthesis of liposomes-templated CdSe hollow and solid nanospheres," *Materials Letters*, vol. 60, no. 1, pp. 11–14, 2006.

[29] J. G. Yu, X. J. Zhao, and Q. N. Zhao, "Photocatalytic activity of nanometer TiO_2 thin films prepared by the sol-gel method," *Materials Chemistry and Physics*, vol. 69, no. 1–3, pp. 25–29, 2001.

[30] Q. Zhang, W. Li, and S. X. Liu, "Controlled fabrication of nanosized TiO_2 hollow sphere particles via acid catalytic hydrolysis/hydrothermal treatment," *Powder Technology*, vol. 212, no. 1, pp. 145–150, 2011.

[31] D.-Y. Choi, J.-Y. Park, and J.-W. Lee, "Adsorption and photocatalysis of spherical TiO_2 particles prepared by hydrothermal reaction," *Materials Letters*, vol. 89, pp. 212–215, 2012.

[32] G. G. Tang, D. Zhang, L. Zhao et al., "Template-free synthesis of uniform TiO_2 mesoporous microspheres with enhanced photocatalytic activity," *Materials Letters*, vol. 118, pp. 192–195, 2014.

[33] F. Mei, C. Liu, L. Zhang et al., "Microstructural study of binary TiO_2:SiO_2 nanocrystalline thin films," *Journal of Crystal Growth*, vol. 292, no. 1, pp. 87–91, 2006.

[34] M. P. Casaletto, G. M. Ingo, S. Kaciulis, G. Mattogno, L. Pandolfi, and G. Scavia, "Surface studies of in vitro biocompatibility of titanium oxide coatings," *Applied Surface Science*, vol. 172, no. 1-2, pp. 167–177, 2001.

[35] G. Li, Z. Q. Liu, Z. Zhang, and X. Yan, "Preparation of titania nanotube arrays by the hydrothermal method," *Chinese Journal of Catalysis*, vol. 30, no. 1, pp. 37–42, 2009.